esa

SP-1290

Microgravity Applications Programme

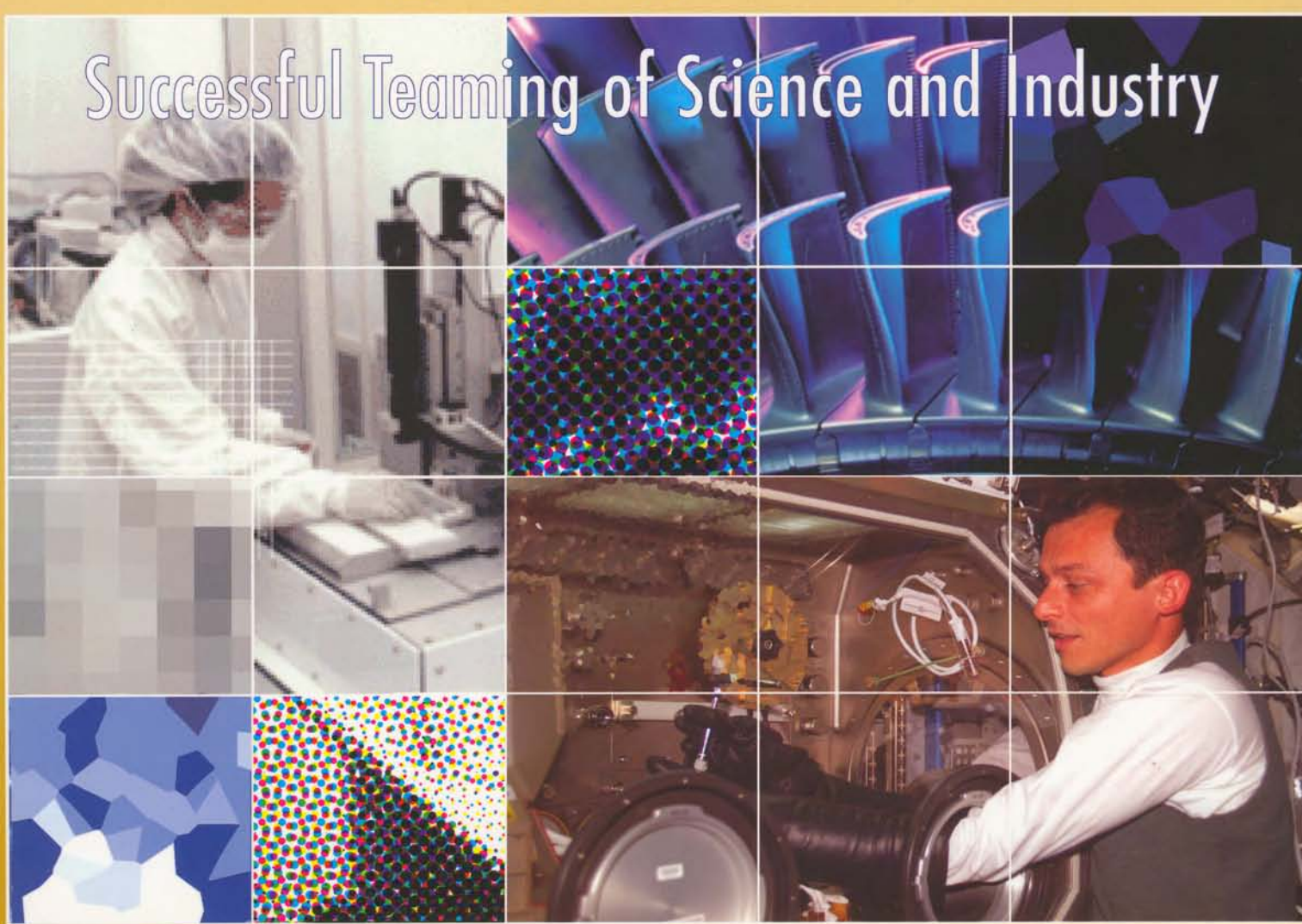

European Space Agency
Agence spatiale européenne

SP-1290
October 2005

Microgravity Applications Programme

Successful Teaming of Science and Industry

European Space Agency
Agence spatiale européenne

SP-1290 'Microgravity Applications Programme: Successful Teaming of Science and Industry'
ISBN 92-9092-971-5 ISSN 0379-6566

Edited by
Andrew Wilson
ESA Publications Division

Coordination
Benny Elmann-Larsen
Directorate of Human Spaceflight,
Microgravity & Exploration

Published by
ESA Publications Division
ESTEC, Noordwijk, The Netherlands

Price
€50

Assessment of Bone Structure and its Changes in Microgravity

Report of the
ESA MAP Team in Biotechnology
2D and 3D Quantification of Bone Structure and its Changes in Microgravity Conditions by Measures of Complexity (MAP AO-99-030)

Loss of bone mass and structure is one of the most prominent risk factors associated with human spaceflight. The main objective of this multifaceted MAP project was therefore to establish a precise diagnostic method for quantifying alterations in the structural composition of human trabecular bone. Tools based on evaluation of 2-D Computed Tomography (CT) and 3-D micro-CT (μCT) images by measures of complexity were developed. These tools quantify different aspects of spatial bone architecture. The measures, methods and results were validated by comparison with conventional histomorphometry and biomechanical testing. In order to visualise the obtained μCT data, special tools had to be developed able to handle huge amounts of data. Additionally, bone models were designed to simulate and predict bone loss, provide test objects for the new structural measures, and gain insight into the effects of mechanical loading on bone structural alterations. A novel ultrasonic methodology for bone structure assessment is in development using the results of experiments into skeletal discordance and new insights in ultrasound technology. The outcome of this comprehensive project will have an impact on health care for space crews as well as for patients with bone diseases on Earth.

1. Introduction

Bone loss is the second highest risk factor (after radiation exposure) of long-duration spaceflights. This MAP project is developing tools to assess alterations in the trabecular bone structure and to gain new quantitative information about bone metabolism under microgravity conditions. This evaluation is based mostly on symbolic dynamics and measures of complexity derived from nonlinear dynamics. A procedure for assessing trabecular bone architecture was developed and scientifically validated by comparison with the current 'gold standard' for bone structural evaluation: histomorphometry. The proposed method can thus be used as a diagnostic tool for assessing the structural alterations of human skeletons during spaceflight. In addition, the ability of the method for predicting compressive vertebral bone strength was assessed.

The objectives of the study were to:

— establish a precise non-invasive diagnostic method for quantification of status and changes in bone structural composition;
— explore the deterioration of human bone tissue in osteoporosis as a model for bone loss under microgravity conditions;
— develop tools to evaluate structural loss in bone architecture and provide new quantitative information about changes in trabecular bone architecture in microgravity.

The outcome of this study is providing the foundation for the monitoring, prevention and treatment of structural changes of bone in microgravity. The results of this project affect the following areas:

— health care for space crews;
— health care for patients with bone diseases on Earth;
— theoretical physics, signal and image analysis, and material science;
— scientific visualisation, interactive visual data analysis, and management of large data sets.

2. Theoretical Background

2.1 Osteoporosis and Bone Loss in Microgravity

During an average lifetime, bone density declines by more than 50% in women, and by more than 30% in men. This decline can decrease below World Health Organisation-defined thresholds and symptoms of osteoporosis, in particular fractures, can occur. Osteoporosis is characterised by decreased bone mass and a deterioration of the micro-architecture leading to increased skeletal fragility (Marx, 2004). It is a highly prevalent disease, affecting approximately 200 million women worldwide, including a third of 60-70 year-olds and two-thirds of those older than 80. Five million osteoporotic women in the US have already suffered fractures. Incidence rates appear to vary sevenfold or more between European countries, which makes it difficult to cite European epidemiological studies, whereas the variation in rates between different localisations in the US is much less (Ross, 1998). Osteopenia, as a precursor to osteoporosis, may occur for various reasons, including immobility, such as bed rest and microgravity.

Since the first manned spaceflights, the problem of muscle and bone atrophy has been evident. The largest changes in bone mass after exposure to microgravity have been found at the load-bearing lower extremities (Vico et al., 2000) and in the axial skeleton (LeBlanc et al., 2000). Although no pathological fractures have yet occurred, spaceflight-related bone loss may potentially have serious consequences in long-duration spaceflight. Recovery is a long process, if achievable at all (Zerath et al., 1996; Lafage-Proust et al., 1998).

2.2 Bone Status Assessment and Structural Measures of Complexity

During spaceflight, the body is exposed to microgravity and thereby to skeletal unloading, which results in skeletal atrophy (Lang et al., 2004; Vico et al., 2000). It has long been recognised, from clinical and animal studies, that immobilisation or skeletal unloading results in a loss of bone mass and bone strength (Allison & Brooks, 1921; Krølner & Toft, 1983; Roux, 1896). It is well known that bone density is a good predictor of compressive bone strength (Bell et al., 1967; Ebbesen, et al., 1999; Mosekilde et al., 1987). However, it has also been suggested that loss of trabecular bone strength and the resulting increased risk of bone fractures also depends on the loss of structural elements and on a loss of connectivity (Kleerekoper et al., 1985; Parfitt, 1987; Mosekilde et al., 1987). Consequently, it is important when investigating pathological, age-related, treatment-induced or immobilisation-induced changes in trabecular bone to ascertain not only the changes in bone density but also the changes in bone structure.

At present, the only method to evaluate trabecular bone structure *in vivo* is via bone biopsies, which is an invasive procedure. The current 'gold standard' for investigating trabecular bone structure is histomorphometry applied to histological sections, which is a destructive evaluation method. Recent advances in micro-computed tomography (μCT) and magnetic resonance imaging (MRI)

have made it feasible to perform 3-D evaluations non-destructively (Feldkamp et al., 1989; Rüegsegger et al., 1996; Wehrli et al., 2002). However, at present these methods still require an invasive extraction of a bone sample from the individual under examination.

Therefore, the main goal of this MAP study was to develop a technique or a series of techniques to evaluate and monitor the trabecular bone structure in a non-invasive and non-destructive manner. The methodology shall be applicable to astronauts so that their skeletal status can be monitored and appropriate countermeasures can be taken if necessary.

Consequently, non-destructive and non-invasive examinations of bone status must be performed by radiological procedures. Pathological alterations of the bone appear as radiological changes in density and structure. Changes in bone mineral density (BMD) can be detected and quantified by several well-established osteodensitometric methods; quantitative computed tomography (QCT) is the standard. In particular, bones of the lower and upper extremities can be examined with peripheral QCT (pQCT).

In order to assess the trabecular bone structure using CT and µCT images, the team proposes that the bone structure follows the rule of a complex system. The origin of this complexity is the hierarchical nature of the bone structure (Olson, 1997; Fratzl, 2004). Complexity characterises a system with many interacting and interrelating components. These various interactions and transactions lead to the emergence of new collective nonlinear properties for the system as a whole (Nature Insight, 2001). The collective behaviour of certain parts of the system implies that this behaviour is a property of the whole system, but not of its single parts. Measures of complexity (Zurek, 1990) are needed in order to quantify different aspects of complex nonlinear systems.

The field of nonlinear dynamics develops and applies such measures of complexity, e.g. for quantification of complex spatial structures. Owing to the increasing quality of µCT data, the focus has recently shifted to the analysis of local curvatures of porous media (Lang et al., 2001; Jinnai et al., 2002).

It has been suggested that fractal dimension increase the ability to predict bone strength (Majumdar et al., 1999) or fracture risk (Benhamou et al., 2001) over that obtained by area BMD alone. However, the merit of fractal dimension is unclear since light microscopy studies have shown that the human trabecular network is not fractal.

Promising techniques proposed for analysis of 1-D or 2-D data are Moran's index, lacunarity, and recurrence plot-based measures. Moran's Index describes spatial autocorrelation in a 2-D plane, while the lacunarity is a measure of the translational invariance of the structure of the object. Their potential has been shown in applications on general 2-D image analysis (Chen et al., 2003) and on investigations of CT or MRI images of bone (Dougherty et al., 2001). Moreover, recent studies of recurrence plot-based methods have paved the way for the development of new complexity measures for the analysis of recurrent structures (Marwan & Kurths, 2005; Romano et al., 2004).

2.3 Visualisation of 3-D Data

Classical tasks of 3-D data visualisation are volume rendering and iso-surface rendering. A comprehensive overview of these visualisation techniques is provided by Hansen & Johnson (2005). As the spatial resolution of CT equipment continues to improve, the need for new techniques for visualisation and exploration of such data increases. Thus a decrease in voxel size by a factor of s results in a growth of the resulting amount of (uncompressed) image data by a factor of s^3. Such increase of data volumes exceeds the technological growth of the capacity of computer main memory.

Therefore, the resulting data sets typically cannot be loaded completely into the main memory of even specialised graphics workstations. This must be taken into consideration when designing a contemporary visualisation system. Such a visualisation system should be able to process spatial data of any size, on any size computer with well scaling performance. In addition, it should allow the user to identify important regions of the data quickly, and then enable focused access to those regions (Law et al., 1999). External memory algorithms and data structures (Vitter, 2001) provide a general framework for addressing these problems. Recent applications in visualisation comprise demand paging (Cox & Ellsworth, 1997) and optimised prefetching for visualisation (Bergeron et al., 2005). Massive data sets are often stored centrally, in data repositories. This dictates a need to access and explore the data remotely via the Internet. Distributed visualisation (Brodlie et al., 2004) tries to meet this need. Various strategies for distributing the visualisation pipeline may be suitable depending on the size of the data and the applied visualisation technique (Luke & Hansen, 2002). Building a practical system for visualisation, remote access and exploration of large data sets is an ongoing research task. In this project, the aim was to build a system that was specifically useful for supporting research on quantification of 3-D trabecular bone structures.

2.4 Quantitative Ultrasound

Quantitative ultrasound (QUS) provides bone quantification without exposure to ionising radiation (Gregg et al., 1997). The majority of bone QUS devices that are lightweight and portable have appeared in the last two decades. They were designed for testing calcanei. However, several modalities of axial QUS intended for the long bones, using unilateral access, were also developed (Hans et al., 1999). The two main parameters used in QUS, either independently or in combination, are the ultrasound velocity (Speed of Sound, SoS) and the slope of the attenuation–frequency curve (Broadband Ultrasonic Attenuation, BUA) (Njeh et al., 1999). The main determinant of the SoS is the stiffness of the material, while the BUA – when measured in trabecular bone – is determined mainly by the scattering properties of the trabecular network. Ultrasound attenuation in trabecular bone is affected by its structure but it also depends on the bone density (Njeh et al, 2001). Current axial techniques are limited by the fact that the longitudinal wave velocity is almost exclusively dependent on the material properties of cortical bone, and is therefore not useful for assessment of trabecular bone. Promising innovations include introduction of new parameters that are sensitive to bone functional properties and their adaptation to new clinically important skeletal sites. Therefore, the aim of the team's research was

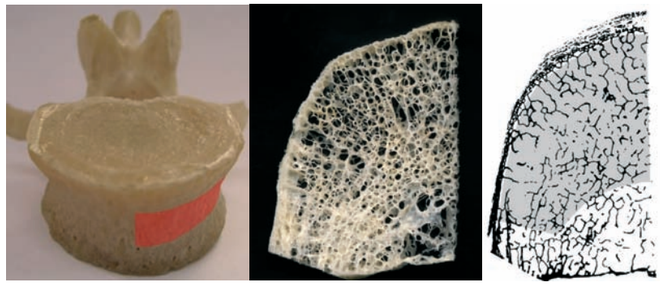

Fig. 1. Left: the region of the vertebral bodies analysed with classical histomorphometry. Centre: a 9 mm-thick central horizontal vertebral bone specimen used for histomorphometry. Right: a 10 µm-thick histological vertebral section with the investigated region of interest (grey) superimposed.

to find a novel ultrasonic approach for the characterisation of the trabecular structure in the proximal tibia.

3. Experiments and Results

3.1 Histomorphometry

At present, static histomorphometry is considered to be the 'gold standard' for assessing the architectural composition of trabecular bone. New methods for assessment of the architecture of cancellous bone have to be verified against this standard. However, in contrast to the proposed CT-based methods, histomorphometry is a destructive and invasive evaluation procedure.

3.1.1 Vertebral Histomorphometry

In order to perform the best possible comparison between histomorphometry and the CT-based measures, the same vertebral region was evaluated by both techniques (Fig. 1). A 9 mm-thick central slice was obtained from half of each of the vertebral bodies. These bone slices were embedded in methylmetacrylate, cut into 10 µm-thick sections, stained with aniline blue and mounted on microscope slides. The bone sections were digitised by scanning at a high resolution (pixel size 10 µm) in a flatbed image scanner with an integrated transparency unit.

The bone architecture was characterised by histomorphometry based on stereological methods. A custom-made fully automated computer program was used to perform the histomorphometric analyses (Thomsen et al., 2000). The analysed region of interest (ROI) corresponded to that used for computation of the 2-D pQCT-based measures of complexity (section 3.3) (Fig. 1). The histomorphometrical analyses included:

- bone volume fraction (BV/TV);
- marrow ($V^*_{m.space}$) and bone ($V^*_{b.space}$) space star volume (Vesterby et al., 1991);
- parallel-plate model (Tb.Th, Tb.N, Tb.Sp) (Parfitt et al., 1983);
- node-strut analysis (Nd/Tm) (Garrahan et al., 1986);
- trabecular bone pattern factor (TBPf) (Hahn et al., 1992);
- connectivity density (CD) (Gundersen et al., 1993).

3.1.2 Tibial Histomorphometry

Cylindrical bone samples with a diameter of 7 mm were obtained perpendicular to the length axis of the tibia 17 mm below the tibial plateau at the medial side of the proximal tibial metaphysis from 24 cadavers (Thomsen et al., 2005a). The histological preparation and the histomorphometrical analyses were performed as described for the vertebral bodies.

3.1.3 Iliac Crest Histomorphometry – Influence of Bedrest on Bone Structure

It is difficult to obtain bone samples from space crews so bedrest studies are used to simulate microgravity in order to study the effects of skeletal unloading on the trabecular architecture. However, undertaking a bedrest study is a major task and is beyond the scope of the present investigation. Instead, the team established a working relationship with the Institute of Biomedical Problems (IMBP) in Russia and gained access to bone sections obtained from test subjects who participated in a 370 day-long bedrest study conducted in the 1980s (Grigoriev et al., 1992).

The part of that study relevant here concerned five test subjects who underwent 5° head-down bedrest for 120 days without countermeasures. Standard iliac crest bone biopsies were obtained before and after this bedrest period. Histomorphometry was performed as described in Section 3.1.1. In these subjects, a significant loss of bone volume fraction and a significant increase of trabecular separation were found. The rate of bone loss was 22 times higher than in similarly aged subjects not undergoing bedrest. In addition, a substantial loss of trabecular number was also detected, whereas trabecular thickness was non-significantly increased (Thomsen et al., 2005b). These results are corroborated by the findings of Palle et al. (1992) and Modlesky et al. (2004). Consequently, this indicates that bedrest- and microgravity-induced bone loss probably functions through a removal of thin trabeculae rather than through an overall thinning of the cancellous bone network.

3.2 Biomechanical Testing

In order to evaluate the abilities of the various structural measures to predict bone strength, it is vital to determine the fracture strength of the examined bone. However, as vertebral histomorphometry and biomechanics are both destructive testing methods, more than one vertebral body is required from each individual. Consequently, the third lumbar vertebral bodies (L3) were used for biomechanical testing, whereas the fourth lumbar vertebral bodies (L4) were used for histomorphometry.

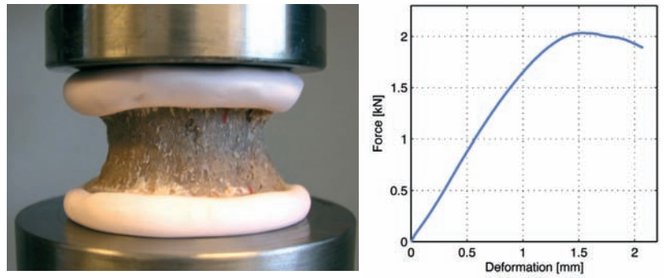

Fig. 2. Left: a vertebral body with interface material at either endplate placed in the materials-testing machine. Right: force-deformation curve originating from the compression testing of one vertebra with interface material attached to both endplates.

An interface material was placed on either side of the vertebral bodies. Before the interface material hardened, the vertebrae were placed in the testing machine and a gentle pressure was applied so that the interface material was distributed evenly over the endplates and thus fitted perfectly to the machine (Fig. 2). The interface material was carefully selected so that its biomechanical properties were similar to those of intervertebral discs (Young's modulus: ~20 MPa).

After the interface material had hardened, the vertebrae were compressed to failure at a constant deformation rate of 5 mm/min. During compression, force and deformation values were automatically recorded (Fig. 2). The failure point is defined as the maximum force applied during the compression. The measured failure force is that of the bone, whereas the measured stiffness is a combination of the stiffness of the bone and the interface material. In order to enable a comparison between individuals of different sizes, the maximum stress values were computed as the maximum force values divided by the average cross-sectional area of the vertebrae.

3.3 2-D Measures of Complexity to Quantify Bone Loss and Estimate Bone Strength from CT and pQCT images

Images acquired with CT and pQCT from different skeletal sites are used for 2-D analysis of loss of bone structure. Normal, osteopenic and osteoporotic specimens were used as a model for bones exposed to

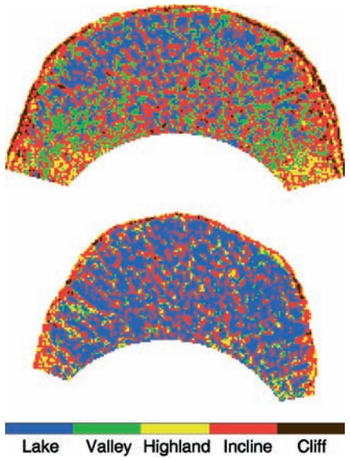

Fig. 3. Standardised and symbol-encoded ROIs of normal (top) and osteoporotic (bottom) vertebrae L4 obtained from mid-axial pQCT slices. Only five different types of symbols are used to represent bone composition.

microgravity. After development, the procedures were adapted to patient examination and are now ready for examination of space crews.

3.3.1 Measures of Complexity Derived from CT Images

The method is based on nonlinear and symbolic dynamics of complex systems. The developed technique is especially advantageous when the CT images are unable to resolve individual trabeculae, and the value of each voxel therefore represents contributions from several structural elements.

The technique consists of three main stages: image preprocessing, image encoding and quantitative structural assessment. The image preprocessing includes calibration, standardised segmentation of the ROI, and a split of the ROI into entire bone, trabecular bone and cortical bone. During image encoding, the attenuation value of each pixel is substituted by one of only five different symbols (Fig. 3). The encoding procedure is based on both the dynamics and the level of X-ray attenuation in the vicinity of an encoded pixel. Finally, the developed set of measures of complexity was used for quantification of different aspects of bone architecture in a holistic way:

- entropy quantifies the probability distribution of X-ray attenuation within the ROI;
- Structure Complexity Index (SCI) assesses the complexity and homogeneity of the structure as a whole;
- Structure Disorder Index (SDI) measures the degree of order/disorder within the bone;
- Trabecular Network Index (TNI) evaluates richness, orderliness and homogeneity of the trabecular network;
- Index of Global Ensemble (IGE) assesses the overall dynamics of the structural elements;
- Maximal L-block and Mean L-block quantify bone tissue replacement by marrow tissue.

In addition, volumetric BMD was calculated using the same ROI. A detailed description of the method can be found in (Saparin et al., 1998; Gowin et al., 2001; Saparin et al., 2002).

3.3.2 Relationship between Measures of Complexity and Histomorphometry

The developed structural measures of complexity were compared with histomorphometry using 26 bone biopsies from the proximal tibia and 23 entire L4. CT-images were acquired by a pQCT scanner (Fig. 4). Despite the fact that the measures of complexity were derived from pQCT images of much lower resolution than the histomorphometric evaluation, very good or excellent correlations were found between the measures of complexity and the appropriate histomorphometric measures (Saparin et al., 2005a). The complexity

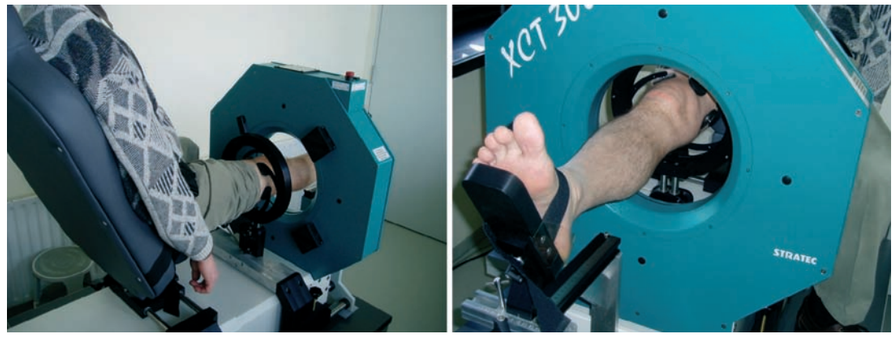

Fig. 4. The Stratec XCT-3000 pQCT scanner adopted for evaluation of bone structure and bone density in proximal tibia. The device can examine the bone status of patients and space crews.

measures can provide information on the bone architecture corresponding to the following histomorphometric parameters: BV/TV, $V^*_{m.space}$, Tb.N, Tb.Sp, Nd/Tm, TBPf and CD. Owing to the pixel size and the slice thickness, the width of a single trabecula cannot be evaluated from 2-D CT images. Therefore, at present information provided by the two histomorphometric measures Tb.Th and $V^*_{b.space}$ cannot be matched by CT-imaging. However, the bedrest study (Section 3.1.3) showed that immobilisation, and therefore probably also microgravity, does not have an impact on Tb.Th, whereas BV/TV and Tb.Sp were significantly affected. Therefore, it is safe to say that the technological limitations of the proposed methodology will have no effect on the results when it is used for the examination of space crews.

3.3.3 Prediction of Bone Strength

The ability of the 2-D CT-based complexity measures to predict bone strength was investigated by performing pQCT scans and compression tests (Section 3.2) on the same human L3 specimens. It was found that the structural measures obtained from the entire bone (trabecular plus cortical) ROI provided higher correlations with failure stress than structural measures obtained from trabecular bone alone. Multiple regression of the bone strength with the complexity measures revealed that these structural measures can explain more than 94% of the variation in vertebral bone strength (Saparin et al., 2005a).

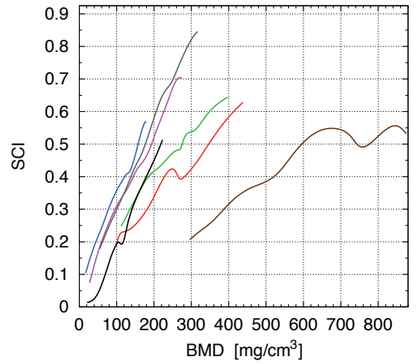

Fig. 5. Structure-density diagram for seven different skeletal locations: structure complexity index SCI versus BMD. The data are approximated by Bézier curves for visualisation purposes. The curves have different slopes characterising the different relations between the density and the complexity of trabecular bone architecture at different skeletal locations. When evaluating a particular BMD-level, such as 200 mg/cm³, the respective complexity of the bone architecture differs considerably from one location to another. Blue: proximal tibia; dark green: femoral head; mauve: calcaneus; black: vertebra L3; light green: femoral neck; red: distal radius; brown: humeral mid-shaft.

3.3.4 Structural Complexity at Different Skeletal Sites and Optimal Location

In order to identify an optimal skeletal location for assessment of the bone structural composition after exposure to microgravity or during osteoporosis, measures of complexity were applied to evaluate seven different skeletal sites: distal radius, humeral midshaft, vertebral body L3, femoral head,

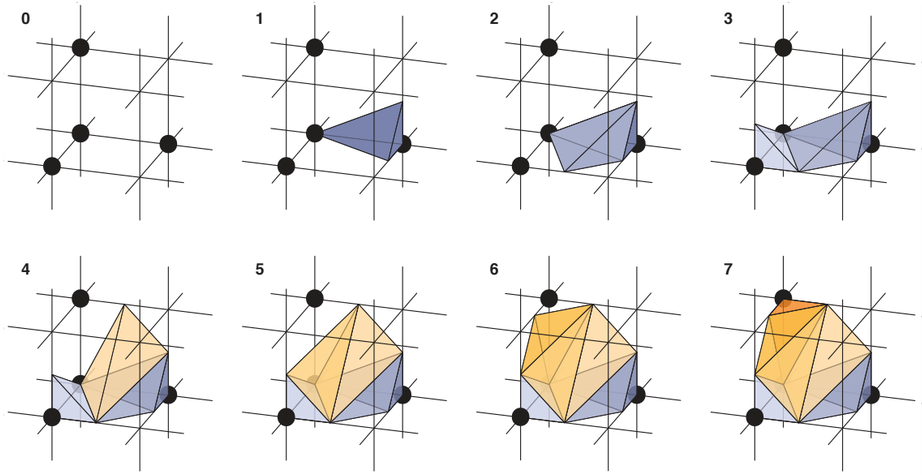

Fig. 6. A marching cube (MC) consists of eight neighbouring voxels, arranged at the corners of the cube. By filling the MC with tetrahedrons, the volume can be better estimated than by counting bone voxels. Moreover, the distinct MC configurations (see text) were used to intoduce a new set of 3-D measures of complexity.

femoral neck, proximal tibia and calcaneus (Saparin et al., 2002). Bone samples were obtained from 29 individuals and examined for each of these skeletal sites. It was shown that bones from different skeletal locations have different structural complexities and different degrees of disorder despite having similar BMD values (e.g. SCI vs. BMD, Fig. 5). The complexity of the bone architecture is much lower in the distal radius and the femoral neck than in the proximal tibia, calcaneus or femoral head although they may have the same BMD value. The normalised slope of the curves in the structure-density diagrams can be used to estimate the relation between the structural differences and the differences in BMD during bone loss. The normalised slope for the radius and the femoral neck is half that of the femoral head, proximal tibia, calcaneus and L3. For the same loss in BMD, the structural complexity of the femoral head, proximal tibia, calcaneus and L3 change twice as fast as at the distal radius and the femoral neck (Fig. 5). The humeral mid-diaphysis consists mainly of cortical bone and therefore behaves differently. Consequently, the skeletal site most suited for monitoring the bone structural status of space crew has to be found from femoral head, proximal tibia, calcaneus and L3.

3.3.5 In Vivo Examination

With support from industrial partner Siemens AG, the developed method was implemented for *in vivo* examination of patients and space crews. This includes CT-imaging of the third lumbar vertebra and CT- or pQCT-imaging of the proximal tibia. The image analysis program includes BMD measurements and quantification of the architectural composition of the bone regions by 2-D measures of complexity. Additionally, a high-resolution and low-radiation pQCT scanner was specially configured for evaluation of the bone structure in the proximal tibia (Fig. 4). A pilot study of healthy volunteers confirmed that the developed technique can differentiate bone architecture from CT- and pQCT-images of proximal tibiae and vertebrae taken *in vivo*.

In addition, L3 and proximal tibia of stroke patients (hemiplegic or paraplegic), patients with a fracture of upper or lower limb, and patients with a rupture of a ligament at the lower limb will be investigated in a longitudinal study with the proposed method. CT-scans will be performed at baseline (trauma), and again 3 and 6 months after baseline.

3.3.6 Conclusions and Recommended Procedure for Bone Status Assessment

Based on the investigations, it was found that the most appropriate procedure for bone status assessment of space crews and patients on Earth includes examination of the lumbar spine and the proximal tibia. Examination of the axial skeleton at the lumbar spine by QCT is already the standard for bone-density assessment. Importantly, the developed evaluation of the bone structure uses the CT-images that can also be used for the BMD assessment, which therefore does not require additional radiation exposure. By combining the BMD evaluation with an evaluation of the structural composition, the best outcome of this non-invasive procedure is obtained.

The lower extremities experience the greatest changes in bone status during exposure to microgravity (Vico et al., 2000) and it is therefore essential to quantify those skeletal changes. The proximal tibia has a very rich trabecular network, which is similar in its behaviour to the vertebral body and is easily accessible. Similar to the lumbar vertebra, both the density and the structural composition will be evaluated at this skeletal site. By comparing the outcome of the axial skeletal examination with the peripheral skeletal examination, any discordance between these two skeletal sites in their response to microgravity exposure will be determined. Such a discrepancy is important for the design and evaluation of individual countermeasures.

The team concludes that the proposed method can assess bone status, quantify structural differences in bone architecture, and can be used as a predictor for vertebral bone strength in a non-invasive and non-destructive manner.

3.4 3-D Structural Analysis with Measures of Complexity

The rapid progress in 3-D µCT resolution facilitates investigations of the micro-architecture of bone and the need for innovative measures for quantifying the 3-D trabecular bone structure has therefore increased. The first approaches have extended traditional 2-D histomorphometry into 3-D (Ito et al., 1998).

Based on the method described in Section 3.3, the symbol-encoding algorithm was modified for 3-D images. Only three different types of symbols (representing soft tissue, internal bone or surface bone voxels) were used to encode the trabecular network. The spatial distributions of local relations between these symbols within the encoded 3-D architecture form the foundation for the structural complexity measures (Saparin et al., 2005b):

— 3-D Normalised Entropy of geometrical locations of bone tissue;
— Structure Complexity Index based on bone volume fraction;
— 3-D Structure Complexity Index;
— Surface Complexity Index and Surface Index of Global Ensemble.

Using this method, it was shown quantitatively that the complexity of the 3-D bone architecture decreases concomitantly with decreasing bone density (Saparin et al., 2005b), which corroborates the findings of the 2-D method (Section 3.3).

New ground was broken with the development of complexity measures that locally evaluate the 3-D shape of the trabeculae. This idea is based on the fact that different 3-D objects of the same volume have different surface areas, depending on

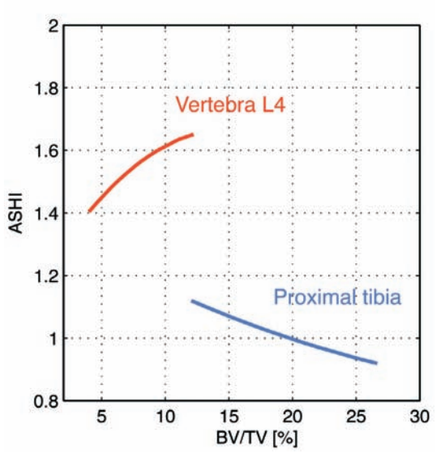

Fig. 7. Averaged Shape Index. This 3-D structural measure of complexity reveals, when applied to trabecular bone of the proximal tibiae and lumbar vertebrae, a clear structural difference between the two skeletal sites owing to the occurrence of more concave structures at the proximal tibia.

their geometrical shape. For example, a long cylinder (length is much larger than radius) has a larger surface than a cube of the same volume, and a sphere of the same volume has the smallest possible surface. The relationship between the measured bone surface area and bone volume is locally determined in a small cubic window that moves through the entire bone. This is used for the definition of several new measures such as Averaged Shape Index (ASHI), Shape Complexity, and Shape Mutual Information. The last two are able to quantify the variety of different shapes, whereas ASHI is able to distinguish rod-like from plate-like structures, and convex from concave structures.

The determination of the local bone surface area and volume is refined by an iso-surface algorithm applied to the 3-D bone data. The most common method for finding the bone volume is to count the bone voxels. A more exact method uses an iso-surface algorithm based on a subset of eight neighbouring voxels arranged at the corners of a cube (Fig. 6; Lorensen & Cline, 1987; Marwan et al., 2005). Such a cube is called a marching cube (MC) and forms the backbone of various iso-surface algorithms for visualisation/rendering of 3-D objects. If two neighbouring voxels of an MC are respectively below and above a predefined threshold value (i.e. one represents bone and another marrow), the iso-surface will lie between these voxels. The iso-surface is then constructed by a set of triangles, and the surface estimation is given by the sum of the areas of these triangles. The bone volume within the MC is filled with tetrahedrons in such a way that the resulting surface is identical to the surface formed by the triangles (Fig. 6). The sum of the volumes of these tetrahedrons is the estimated bone volume found in the MC.

Furthermore, depending on the position of the bone voxels in an MC and by taking rotational symmetry into consideration, there are only 21 unique MC cases possible. Each MC case represents a specific bone surface configuration. Therefore, the distribution of MC cases can be used for defining structural measures of complexity. Consequently, the team developed the MC Entropy Index and the MC Complexity, which quantify the complexity of the bone surface.

In this MAP project, other approaches for assessing the micro-architecture are also being investigated. This includes the extension of 1-D or 2-D data analysis tools based on nonlinear dynamics such as recurrence plots, lacunarity, Moran's index and curvature-based measures.

All these new measures are used for the assessment of structural differences in 3-D trabecular bone architecture. The bone biopsies from the proximal tibia and the entire vertebrae (Section 3.1) were µCT-scanned by Scanco Medical AG (Section 3.5). Standardised volumes of interest (VOI) were applied to the µCT images for quantification of the 3-D architecture. The VOI for the proximal tibial biopsies was a 10 mm-long cylinder with a diameter of 6 mm, located

Fig. 8. 3-D rendering of the skeleton of a proximal tibia biopsy. Rod-like structures are rendered as lines, plate-like structures are represented as central surfaces. The thickness of the structure is colour-coded as saturation.

5 mm below the cortical shell. The VOI for the vertebra was a 25 x 15 x 10 mm cuboid with the centre shifted 4.5 mm backwards from the centre of the vertebra along its symmetry line. The structural measures of complexity based on symbolic dynamics, shape and marching cubes were then computed from these VOIs.

A comparison of these 3-D structural measures with the results of histomorphometry and compression tests reveals good or high correlations between the 3-D structural measures and the appropriate histomorphometric measures and bone strength. The 3-D structural measures are able to assess different aspects of the bone structure and quantify its architectural differences. It can be inferred that compressive bone strength is in general related to more homogeneous bone, higher complexity of the bone surface, thicker trabeculae and well-connected trabecular bone. The shape-related measures such as ASHI clearly differentiated the trabecular structure of the proximal tibia from the lumbar vertebra (Fig. 7). In the proximal tibia, the trabecular network consists mainly of concave structures, whereas in the lumbar vertebra the trabecular bone is mainly formed by convex structures.

The proposed new structural measures of complexity can be used for evaluation of 3-D µCT data sets. They provide a nonlinear holistic quantification of the amount, distribution, shape, connectivity and structural complexity of trabecular architecture and can be used to describe osteoporosis-induced architectural differences.

Based on data from this study, it is concluded that the technique is able to

Fig. 9. 3-D volume rendering of an entire human vertebral body and its trabecular structure (voxel size 38 µm).

quantify alterations in bone architecture and may help to diagnose and monitor changes in bone structure of Earth patients and space crews. It has been agreed that the team will have access to 3-D bone imaging data of astronauts at the end of 2005.

3.5 3-D Visualisation and Analysis of Large Data Sets: Fractures and 3-D Vertebral Architecture.

3.5.1 Visualisation of µCT Data

During the project, the team acquired a large collection of 3-D µCT data sets. Data acquisition was performed by industrial partner Scanco Medical AG. Proximal tibial bone biopsies were µCT-scanned in a Scanco µCT 40 scanner at a voxel size of 20 µm (Thomsen et al., 2005). Entire vertebral bodies were µCT-scanned in a Scanco µCT 80 scanner before and after failure load testing at a voxel size of 38 µm. The sizes of the acquired 3-D images were 2048x2048x1000 voxels at 2 Bytes, resulting in roughly 8 GB of data per specimen. More than 100 such data

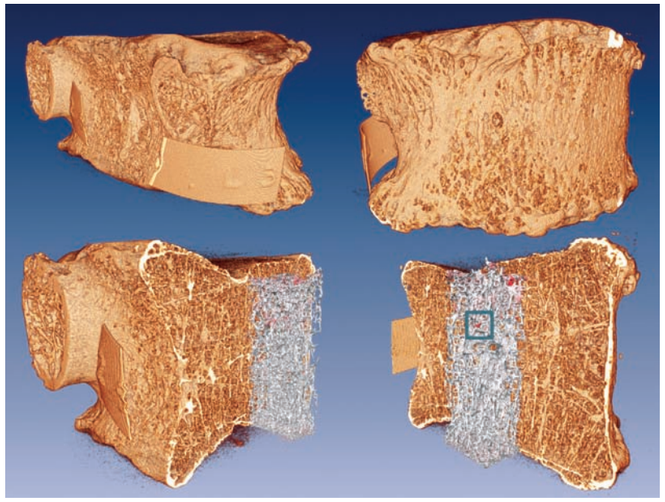

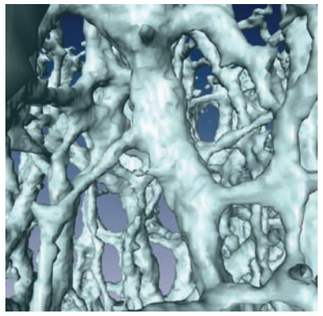

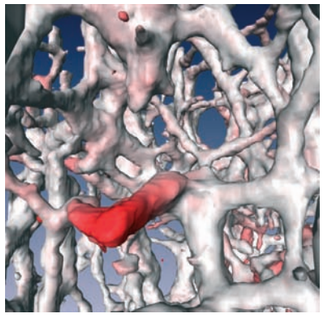

Fig. 10. Micro-fracture of the trabecular network in a vertebral body. Different views of the entire vertebral volume are displayed at the top. The trabecular structure before (left) and after (right) failure load testing is displayed in the bottom row. Structural changes are highlighted in red. A micro-fracture is located in the centre of the right image. The fracture detection procedure is based on the calculation of surface distances.

sets were acquired and transferred to the project server.

A major goal of the project was to match and compare images from different sources for validation and to facilitate the development of new assessment methods. Interactive visualisation for exploration and identification of sub-volumes for further detailed analysis was considered to be crucial. An efficient visualisation algorithm for central surfaces (skeletons) of the trabecular structure (Prohaska & Hege, 2002) was developed and integrated in the advanced visualisation system Amira (Stalling et al., 2005) (Fig. 8). These facilities are now available as extensions to the commercial version of Amira.

3.5.2 Visual Analysis of Large Data Sets

Owing to the large volume of data, administrative tasks such as data allocation and backup had to be performed at one institution only. Thus, it was decided to store the µCT scans centrally in a data repository. Visualisation methods were extended to allow remote access and handling of data exceeding the size of available computer main memory. The entire vertebral bodies could thereby be visualised, including their trabecular structure (Fig. 9). Sub-volumes can be selected interactively for further analysis. The other team institutions have efficient access to the data via the Internet (Prohaska et al., 2004).

3.5.3 Vertebral Structure Before and After Compression Tests

Comparing trabecular micro-architecture of vertebral bodies before and after compression testing (Section 3.2) based on two µCT scans is ongoing research. A manual procedure to perform such comparisons was established. Matching reference points (landmarks) are selected in the scans and utilised to place the scans semi-automatically in a common coordinate system. The two structures may then be manually compared. Sub-volumes can be selected and any of the visualisation techniques available in Amira can be applied, including volume rendering, iso-surfaces and slicing. This comparison is supported through highlighting regions containing changes in the trabecular structure detected by various approaches. The distance between the surfaces of the trabecular structures and the voxel-based difference in the µCT data was successfully used by the project team to detect vertebral micro-fractures (Fig. 10).

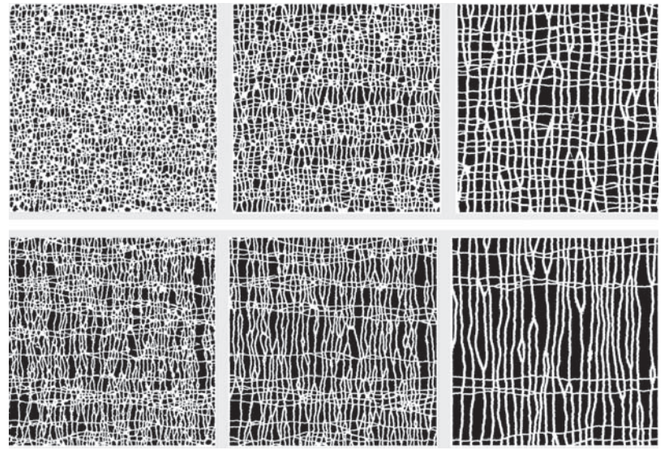

Fig. 11. Two different time evolutions of the model (in 2-D). The sensitivity of osteoblasts to the mechanical stimulus is reduced in the bottom row compared to the simulation of the top row. Both simulations begin with a random configuration of high bone volume fraction. Bone matrix is indicated white, marrow black.

This procedure is the foundation for further research and will be further developed as described in the new MAP proposal (Section 4). Classifying changes in the microscopic structure and deriving a representation summarising the overall change of the vertebrae are short-term goals. Development of a fully automated procedure is a long-term goal, outlined in the next MAP proposal.

3.6 Simulation of Bone Remodelling

Living bone is continuously remodelled by specialised cells. The remodelling process is characterised by an intriguing duality concerning the mechanical performance of bone (Heaney, 2003). Bone remodelling has a long-term positive effect because it removes microdamages from the bone and fatigue fractures are therefore avoided. On the other hand, the ongoing remodelling process itself is a source of trabecular structural weakness owing to the resorption cavities. Not only the bone architecture but also the turnover rate is thought to play a key role in determining the mechanical quality of bone. This demonstrates the importance of a 'dynamic' view of bone. The dynamics of bone modelling and remodelling is the source for adaptive abilities of the bone tissue to changing loading conditions.

This is further corroborated by the fact that the remodelling process is mechanically controlled, which allows bone to adapt to changes in its loading pattern. The Wolff-Roux law states that bone is removed where mechanically not needed and deposited where the local loading is high (Hart, 2001). This principle is realised by several cellular and biochemical feedback mechanisms. For all the current difficulties of experiments with living animals and human beings and the unclear significance of *in vitro* experiments, computer models have been successfully used to test and extend our understanding of the remodelling process.

As a first step, the team has developed several simplified algorithms to simulate bone loss using 2-D and 3-D CT images. The aim was to extrapolate and predict the bone loss and to provide test objects for the measures of complexity. The team developed and tested a threshold algorithm and a virtual slicing algorithm for 2-D images. The threshold algorithm simulates bone resorption on the boundary between bone and marrow, representing activity of osteoclasts. The virtual slicing algorithm uses a distribution of the bone material between several virtually-created slices to achieve statistically correct results, when the bone-marrow transition is not clearly defined. For 3-D data, a variation of the threshold algorithm was developed and applied to µCT data. The results of modelling were compared with real CT images using structural measures of complexity in 2-D and 3-D (Zaikin et al., 2005).

Implementing a specific formulation of the Wolff-Roux law in a computer model and by the use of finite element methods, it was demonstrated that an optimised trabecular

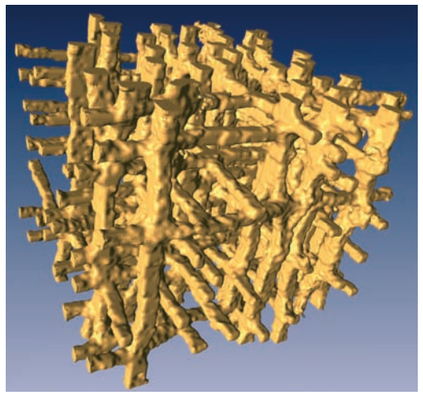

Fig. 12. Snapshot of the 3-D structure that emerged from a random configuration of high bone volume fraction. For the remodelling rule, a step function was assumed that corresponds to an on/off control for the osteoblasts.

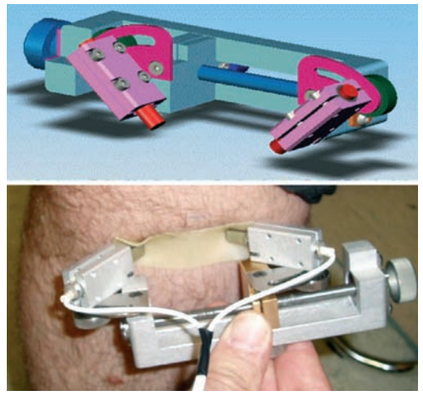

Fig. 13. Laboratory ultrasonic probe for proximal tibia: design (top); probe positioned on volunteer's tibia (bottom).

architecture emerges, which is maintained and adapts to varying loads (Ruimerman et al., 2005). In our model, the trabecular structure inside a human vertebra is mapped on a lattice. The mechanical assessment is performed using a simplified painting algorithm yielding the volume change of each bone element in the structure (Weinkamer et al., 2004). In order to perform changes in the structure, a remodelling rule has to be defined that specifies the probability for depositing or removing a bone element from the bone surface as a function of the local deformation.

Starting the simulations with a homogeneous configuration of a high bone volume fraction, a network-like structure with preferentially vertical and horizontal trabeculae emerged (Fig. 11). A general feature of the model is that the bone volume fraction attained a steady-state value. However, the architecture coarsened with a decreasing number of trabeculae, and a concomitant increase in the thickness of the remaining trabeculae (Weinkamer et al., 2004). Small changes in the mechanosensitivity of the cells changed the trabecular structure significantly (Weinkamer et al., 2005) (Fig. 11).

In addition, real structural data of human vertebrae obtained by µCT was used as initial conditions for the model. A single triaxial loading mode was applied to the system. Under this loading condition, the complex trabecular structure rapidly simplified with only a few but thick trabeculae remaining. Apart from the simple mechanical description in the model, the main reason for this rapid simplification is the uniform loading of the system. Daily activities of a human being lead to a more complex (but unknown) loading pattern of the spine, which presumably together with the particular biomechanical properties of the intervertebral discs plays a role in sustaining the complexity of the vertebral architecture.

The team's research now focuses on the interrelation between the control of the remodelling process reflected in the remodelling rule and the resulting architecture (Fig. 12). Already very subtle changes in the remodelling rule can change the morphology and the time evolution of the structure. An example is the changes induced in the structure by alterations in how the remodelling rule for the total cell action is distributed to osteoclasts and osteoblasts.

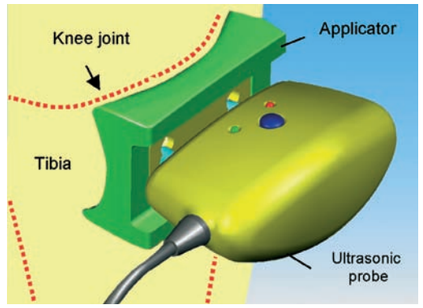

Fig. 14. General view of the proposed ultrasonic probe for human studies.

3.7 Ultrasound Testing of Proximal Tibia for Quantification of Bone Structure

The project team has proposed the proximal tibial metaphysis as a new site for ultrasonic assessment of structural changes in trabecular bone. The advantages of this skeletal site are:

- it is load-bearing bone tissue usually suffering in microgravity (Vico et al., 2000);
- it is mainly composed of trabecular bone and is a highly structured porous medium, where loss of bone mass is tightly bound with changes of the structure;
- it offers easy unilateral access to the examination site.

These properties make the proximal tibia an excellent site for examination of osteopenic and osteoporotic patients.

Low-frequency quasi point-contact transducers and adjustable base probes were designed for *in vitro* and *in vivo* ultrasonic measurements of the proximal tibia by surface transmission (Fig. 13). Propagation signals generated by 0.1 MHz and 0.3 MHz tone-burst waveforms (Tatarinov & Sarvazyan, 2003) and continuous-frequency sweeps in the 0.1-0.5 MHz band were acquired during transmission of the combined signal packet and were analysed.

The method was developed and validated on 41 proximal tibial specimens, including normal, osteopenic and osteoporotic bone. In addition, its sensitivity to structural differences in objects of similar densities was tested with different specially designed phantoms (Tatarinov et al., 2005). It was found that the proposed ultrasonic parameters are able to detect and quantify differences in internal scatterers even when the density of the phantoms was kept constant. Finally, the feasibility of obtaining ultrasonic responses from *in vivo* bones through layers of soft tissue was demonstrated by examination of healthy volunteers.

The team suggests the following methods and parameters for quantification of bone architecture: ultrasonic spectra and its derivatives; frequency slope and shifts of peak frequencies; group velocities of characteristic wave packets; logarithmic damping coefficient of the broadband signal normalised with the propagation distance; pulse dissipation (dispersion).

It was found that several of the proposed ultrasonic parameters were able to assess the status and detect the differences in the bone structure (Tatarinov et al., 2005). High frequencies were prevailing in osteoporotic bones. Sweep responses showed different relative intensities of the 0.1 and 0.3 MHz spectral peaks in bones with either high or low trabecular BMD. A good agreement was thus established between the ratio of these intensities and trabecular bone status. A low number of scattering elements (trabeculae) in bones with low trabecular BMD resulted in weaker attenuation of ultrasound in the entire frequency band. Additionally, normal and osteoporotic bone could be discriminated by their dispersion of

propagating wave packets. At low frequencies (0.1 MHz), at least two different wave modes with different group velocities were recorded. The second (slow) wave packet propagated faster in normal bone compared with osteoporotic bone, while there was no significant difference in propagation velocity of the first wave packets.

A prototype of a probe for future human studies at the proximal tibia is illustrated in Fig. 14. In order to complete the design of the ultrasonic device for evaluation of bone status in the proximal tibia, the following remaining issues must be addressed: contact standardisation; adaptation to the proximal tibial anatomy; precise positioning; and elimination of soft-tissue artefacts. The team is confident that addressing the issue of coupling contact standardisation will make the method space-ready.

4. Future Studies

The results of this project are providing the foundation for the quantitative monitoring, assessment of countermeasures, and evaluation of treatment results for structural changes in bone caused by metabolic diseases or exposure to microgravity. In particular, in the future the developed method will be used to evaluate 3-D data of astronauts' extremities when these data become available. The trabecular structure of astronauts' bones is to be evaluated before and after spaceflight by use of a specially developed *in vivo* µCT scanner.

The project team has prepared a new project proposal: 'Assessing the Influence of Microarchitecture on the Mechanical Performance of Bone and its Changes in Microgravity from *In Vivo* Measurements', which was approved by the independent review board. Industry partners Scanco Medical AG, Siemens AG and Siemens Medical Solutions also support the new study. This project will logically continue and substantially extend the current research, raising it to a new level of understanding of the relation between bone architecture and its mechanical properties.

Acknowledgments

This study was made possible by grants from ESA. The project team acknowledges Scanco Medical AG, Siemens AG, and Roche Pharmaceuticals for supporting the study. The team thanks G. Bogusch, Institute of Cell Biology and Neurobiology, Centre for Anatomy, Charité Berlin, Germany, and R. Graf, Institute of Vegetative Anatomy (former Anatomical Institute of Free University Berlin), Center for Anatomy, Charité Berlin, Germany, for providing the bone specimens. The team is grateful for the technical assistance of M. Giehl, E. May and M. Kratzsch, Campus Benjamin Franklin, Charité Berlin, for the processing and CT-imaging of bone specimens, and of I.V. Magnussen, Department of Connective Tissue Biology, Institute of Anatomy, University of Aarhus, Denmark, for preparing the histological sections. A. Laib and M. Burkhart, Scanco Medical AG, Switzerland, are acknowledged for their µCT scanning of the bone samples. B. V. Morukov, Institute of Biomedical Problems (IMBP), Moscow, Russia, L. Vico and C. Alexandre, Laboratoire de Biologie du Tissu Osseux, Faculté de Médecine, Saint-Etienne, France, are acknowledged for scientific cooperation and for providing and preparing the histological sections of the iliac bone specimens from the bedrest study. The team is grateful to M. Hartman, Max Planck Institute of Colloids and Interfaces, Potsdam, Germany for computational work on simulation of bone remodelling. The project team acknowledges Mercury Computer Systems GmbH, Germany for providing the licenses for the Amira software.

References

Allison, N. & Brooks, B. (1921). Bone Atrophy. An Experimental and Clinical Study of the Changes in Bone Which Result from Non-Use. *Surg. Gynecol. Obstet.* **33**, 250-260.

Bell, G.H., Dunbar, O., Beck, J.S. & Gibb, A. (1967). Variations in Strength of Vertebrae with Age and Their Relation to Osteoporosis. *Calcif. Tissue Res.* **1**, 75-86.

Benhamou, C.L., Poupon, S., Lespessailles, E., Loiseau, S., Jennane, R., Siroux, V., Ohley, W. & Pothuaud, L. (2001). Fractal Analysis of Radiographic Trabecular Bone Texture and Bone Mineral Density: Two Complementary Parameters Related to Osteoporotic Fractures. *J. Bone Miner. Res.* **16**, 697-704.

Bergeron, R.D., Rhodes, P.J., Sparr, T.M., & Tang, X. (2005). Out of Core Visualization Using Iterator Aware Multidimensional Prefetching. *Proc. SPIE, Visualization and Data Analysis 5669*, 295-306.

Brodlie, K.W., Duce, D.A., Gallop, J.R., Walton, J.P.R.B . & Wood, J.D. (2004). Distributed and Collaborative Visualization. *Computer Graphics Forum* **23**, 223-251.

Chen, T.-J., Chuang, K.-S., Wu, J., Chen, S.C., Hwang, I.-M. & Jan, M.-L. (2003). A Novel Image Quality Index using Moran I Statistics. *J. Dig. Imag.* **16**, 210-215.

Cox, M. & Ellsworth, D. (1997). Application-Controlled Demand Paging for Out-of-Core Visualization. *Proc. IEEE Visualization '97* 235-244.

Dougherty, G. & Henebry, G.M. (2001). Fractal Signature and Lacunarity in the Measurement of the Texture of Trabecular Bone in Clinical CT Images. *Med. Eng. Phys.* **23**, 369-380.

Ebbesen, E.N., Thomsen, J.S., Beck-Nielsen, H., Nepper-Rasmussen, H.J. & Mosekilde, Li. (1999). Lumbar Vertebral Body Compressive Strength Evaluated by Dual-Energy X-Ray Absorptiometry, Quantitative Computed Tomography, and Ashing. *Bone* **25**, 713-724.

Feldkamp, L.A., Goldstein, S.A., Parfitt, A.M., Jesion, G. & Kleerekoper, M. (1989). The Direct Examination of Three-Dimensional Bone Architecture in Vitro by Computed Tomography. *J. Bone Miner. Res.* **4**, 3-11.

Fratzl, P. (2004). Hierarchical Structure and Mechanical Adaptation of Biological Materials. In *Lecture Notes NATO-ASI on Learning from Nature How to Design New Implantable Biomaterials* (Eds. R.L Reis & S. Weiner), 15-34.

Garrahan, N.J., Mellish, R.W.E. & Compston, J.E. (1986). A New Method for the Two-Dimensional Analysis of Bone Structure in Human Iliac Crest Biopsies. *J. Microsc.* **142**, 341-349.

Gowin, W., Saparin, P., Kurths, J. & Felsenberg, D. (2001). Bone Architecture Assessment with Measures of Complexity. *Acta Astronaut.* **49**, 171-178.

Gregg, E.W., Kriska, A.M., Salamone, L.M., Roberts, M.M., Anderson, S.J., Ferrell, R.E., Kuller, L.H. & Cauley, J.A. (1997). The Epidemiology of Quantitative Ultrasound: A Review of the Relationships With Bone Mass, Osteoporosis and Fracture Risk. *Osteoporos. Int*. **7**, 89-99.

Grigoriev, A.I., Morukov, B.V., Oganov, V.S., Rakhmanov, A.S. & Buravkova, L.B. (1992). Effects of Exercise and Bisphosphonate on

Mineral Balance and Bone Density During 360 Day Antiorthostatic Hypokinesia. *J. Bone Miner. Res.* **7**, S449-S455.

Gundersen, H.J.G., Boyce, R.W., Nyengaard, J.R. & Odgaard A. (1993). The ConnEulor: Unbiased Estimation of Connectivity Using Physical Disector Under Projection. *Bone* **14**, 217-222.

Hahn, M., Vogel, M., Pompesius-Kempa, M. & Delling, G. (1992). Trabecular Bone Pattern Factor – A New Parameter for Simple Quantification of Bone Microarchitecture. *Bone* **13**, 327-330.

Hans, D., Fan, B. & Fuerst, T. (1999). Non-Heel Quantitative Ultrasound Devices. In *Quantitative Ultrasound: Assessment of Osteoporosis and Bone Status* (Eds. Njeh, C.F., Hans, D., Fuerst, T., Glüer C.C. & Genant, H.K.), Martin Dunitz Ltd., pp145-162.

Hansen, C.D. & Johnson, C.R. (2005). *The Visualization Handbook*, Elsevier, The Netherlands.

Hart, R. T. (2001). Bone Modelling and Remodeling: Theories and Computation. In *Bone Mechanics Handbook* (Ed. Cowin, S.C.), CRC Press, pp1-42 (Chapter 31).

Heaney, R.P. (2003). Remodeling and Skeletal Fragility. *Osteoporos. Int.* **14**, S12-S15.

Ito, M., Nakamura, T., Matsumoto, T., Tsurusaki, K. & Hayashi, K. (1998). Analysis of Trabecular Microarchitecture of Human Iliac Bone Using Microcomputed Tomography in Patients With Hip Arthrosis With or Without Vertebral Fracture. *Bone* **23**, 163-169.

Jinnai, H., Watashiba, T., Kajihara, Y., Nishikawa, M., Takahashi, M. & Ito, M. (2002). Surface Curvatures of Trabecular Bone Microarchitecture. *Bone* **30**, 191-194.

Kleerekoper, M., Villanueva, A.R., Stanciu, J., Sudhaker Rao, D. & Parfitt, A.M. (1985). The Role of Three-Dimensional Trabecular Microstructure in the Pathogenesis of Vertebral Compression Fractures. *Calcif. Tissue Int.* **37**, 594-597.

Krølner, B. & Toft, B. (1983). Vertebral Bone Loss: An Unheeded Side Effect of Therapeutic Bed Rest. *Clin. Sci.* **64**, 537-540.

Lafage-Proust, M.H., Collet, P., Dubost, J.M., Laroche, N., Alexandre, C. & Vico, L. (1998). Space Related Bone Mineral Redistribution and Lack of Bone Mass Recovery after Reambulation in Young Rats. *Am. J. Physiol.* **274**, 324-334.

Lang, C., Ohser, J. & Hilfer, R. (2001). On the Analysis of Spatial Binary Images. *J. Microsc.* **203**, 303-313.

Lang, T., LeBlanc, A., Evans, H., Lu, Y., Genant, H. & Yu A. (2004). Cortical and Trabecular Bone Mineral Loss from the Spine and Hip in Long-Duration Spaceflight. *J. Bone Miner. Res.* **19**, 1006-1012.

Law, C., Schroeder, W.J., Martin, K.M. & Temkin, J. (1999). A Multi-Threaded Streaming Pipeline Architecture for Large Structured Data Sets. In *Proc. IEEE Visualization '99*, 225-232.

LeBlanc, A., Schneider, V., Shackelford, L., West, S., Oganov, V., Bakulin, A. & Voronin, L. (2000). Bone Mineral and Lean Tissue Loss after Long Duration Space Flight. *J. Musculoskel. Neuron. Interact.* **1**, 157-160.

Lorensen, W.E. & Cline, H.E. (1987). Marching Cubes: A High Resolution 3D Surface Construction Algorithm. *SIGGRAPH Comput. Graph.* **21**, 163-169.

Luke, E.J. & Hansen, C.D. (2002). Semotus Visum: A Flexible Remote Visualization Framework. *Proc. IEEE Visualization '02*, 61-68.

Majumdar, S., Lin, J., Link, T., Millard, J., Augat, P., Ouyang, X., Newitt, D., Gould, R., Kothari, M. & Genant, H. (1999). Fractal Analysis of Radiographs: Assessment of Trabecular Bone Structure and Prediction of Elastic Modulus and Strength. *Med. Phys.* **26**, 1330-1340.

Marwan, N. & Kurths, J. (2005). Line Structures in Recurrence Plots. *Phys. Lett. A* **336**, 349-357.

Marwan, N., Saparin, P., Thomsen, J.S., Kurths, J. (2005). An Innovative Approach for the Assessment of 3D Structures in Trabecular Bone. *J. Grav. Physiol.;* in Press.

Marx, J. (2004). Coming to Grips with Bone Loss. *Science* **305**, 1420-1422.

Modlesky, C.M., Majumdar, S., Narasimhan, A. & Dudley, G.A. (2004). Trabecular Bone Microarchitecture is Deteriorated in Men With Spinal Cord Injury. *J. Bone Miner. Res.* **19**, 48-55.

Mosekilde, Li., Mosekilde, Le. & Danielsen, C.C. (1987). Biomechanical Competence of Vertebral Trabecular Bone in Relation to Ash Density and Age in Normal Individuals. *Bone* **8**, 79-85.

Nature Insight (2001). Complex Systems. *Nature* **410**, 241-284.

Njeh, C.F., Nicholson, P.H.F. & Langton, C.M. (1999). The Physics of Ultrasound Applied to Bone. In *Quantitative Ultrasound: Assessment of Osteoporosis and Bone Status* (Eds. Njeh, C.F., Hans, D., Fuerst, T., Glüer, C.C. & Genant, H.K.), Martin Dunitz Ltd., pp67-76.

Njeh, C.F., Fuerst, T., Diessel, E. & Genant, H.K. (2001). Is Quantitative Ultrasound Dependent on Bone Structure? A Reflection. *Osteoporos. Int.* **12**, 1-15.

Olson, G. B. (1997). Computational Design of Hierarchically Structured Materials. *Science* **277**, 1237-1242.

Palle, S., Vico, L., Bourrin, S. & Alexandre, C. (1992). Bone Tissue Response to Four-Month Antiorthostatic Bedrest: A Bone Histomorphometric Study. *Calcif. Tissue. Int.* **51**, 189-194.

Parfitt, A.M., Mathews, C.H.E, Villanueva, A.R., Kleerekoper, M., Frame, B. & Rao, D.S. (1983). Relationships between Surface, Volume, and Thickness of Iliac Trabecular Bone in Aging and Osteoporosis: Implications for the Microanatomic and Cellular Mechanisms of Bone Loss. *J. Clin. Invest.* **72**, 1396-1409.

Parfitt, A.M. (1987). Trabecular Bone Architecture in the Pathogenesis and Prevention of Fracture. *Am. J. Med.* **82**, 68-72.

Prohaska, S., & Hege, H.-C. (2002). Fast Visualization of Plane-Like Structures in Voxel Data. In *Proc. IEEE Visualization '02*, 29-36.

Prohaska, S., Hutanu, A., Kähler, R., & Hege, H.-C. (2004). Interactive Exploration of Large Remote Micro-CT Scans. In *Proc. IEEE Visualization '04*, 345-352.

Romano, M., Thiel, M., Kurths, J. & von Bloh, W. (2004). Multivariate Recurrence Plots. *Phys. Lett. A* **330**, 214-223.

Ross P.D. (1998) Epidemiology of Osteoporosis. In *Bone Densitometry and Osteoporosis* (Eds. H.K. Genant,G. Guglielmi & M. Jergas), Springer, pp21-42.

Roux, W. (1896). Ueber die Dicke der statischen Elementartheile und die Maschenweite der Substantia spongiosa der Knochen. *Z. Orthop. Chir.* **4**, 284-306.

Rüegsegger, P., Koller, B. & Müller, R. (1996). A Microtomographic System for the Nondestructive Evaluation of Bone Architecture. *Calcif. Tissue Int.* **58**, 24-29.

Ruimerman, R., Hilbers, P., van Rietbergen, B. &

Huiskes, R. (2005). A Theoretical Framework for Strain-Related Trabecular Bone Maintenance and Adaptation. *J. Biomech.* **38**, 931-941.

Saparin, P., Gowin, W., Kurths, J. & Felsenberg, D. (1998). Quantification of Cancellous Bone Structure Using Symbolic Dynamics and Measures of Complexity. *Phys. Rev. E* **58**, 6449-6459.

Saparin, P., Gowin, W. & Felsenberg, D. (2002). Comparison of Bone Loss with Changes of Bone Architecture at Six Different Skeletal Sites Using Measures of Complexity. *J. Gravit. Physiol.* **9**, 177-178.

Saparin, P., Thomsen, J.S., Beller, G. & Gowin, W. (2005a). Measures of Complexity to Quantify Bone Loss and Estimate Strength of Human Lumbar Vertebrae: Comparison of CT Image Analysis with Bone Histomorphometry and Biomechanical Tests. *J. Gravit. Physiol.*; in Press.

Saparin, P., Thomsen J.S., Prohaska, S., Kurths, J., Zaikin, A., Hege, H.-C., Gowin, W. (2005b). Quantification of Spatial Structure of Human Proximal Tibial Bone Biopsies Using 3D Measures of Complexity. *Acta Astronautica* **56**, 820-830.

Stalling, D., Westerhoff, M. & Hege, H.-C. (2005). Amira: A Highly Interactive System for Visual Data Analysis. In *The Visualization Handbook* (Eds. Hansen, C.D. & Johnson, C.R.), Elsevier, The Netherlands, pp749-767.

Tatarinov, A. & Sarvazyan, A. (2003). Dual-Fequency Method for Ultrasonic Assessment of Bones: Model Study. In *Proc. World Congress Ultrasonics, Paris*, CDROM, 895-898.

Tatarinov, A., Gowin, W., Beller, G. & Saparin, P. (2005). A Perspective for Ultrasonic Assessment of Osteoporotic Changes of Bone Structure in Proximal Tibia. *J. Gravit. Physiol.;* in Press.

Thomsen, J.S., Ebbesen, E.N. & Mosekilde, Li. (2000). A New Method of Comprehensive Static Histomorphometry Applied on Human Lumbar Vertebral Cancellous Bone. *Bone* **27**, 129-138.

Thomsen, J.S., Laib, A., Koller, B., Prohaska, S., Mosekilde, Li. & Gowin, W. (2005a). Stereological Measures of Trabecular Bone Structure: Comparison of 3D Micro Computed Tomography with 2D Histological Sections in Human Proximal Tibial Bone Biopsies. *J. Microsc.* **218**, 171-179.

Thomsen, J.S., Morukov, B.V., Vico, L., Alexandre, C., Saparin, P.I. & Gowin, W. (2005b). Cancellous Bone Structure of Iliac Crest Biopsies following 370 Days of Head-Down Bed Rest. *Aviation Space Environ. Med.*; in Press.

Vesterby, A., Mosekilde, Li., Gundersen, H.J.G., Melsen, F., Mosekilde, Le., Holme, K. & Sørensen, S. (1991). Biological Meaningful Determinants of the In Vitro Strength of Lumbar Vertebrae. *Bone* **12**, 219-224.

Vico, L., Collet, P., Guignandon, A., Lafage-Proust, M.-H., Thomas, T., Rehailia, M. & Alexandre, C. (2000). Effects of Long-Term Microgravity Exposure on Cancellous and Cortical Weight-Bearing Bones of Cosmonauts. *Lancet* **355**, 1607-1611.

Vitter, J. S. (2001). External Memory Algorithms and Data Structures: Dealing with Massive Data. *ACM Computing Surveys* **33**, 209-271.

Wehrli, F.W., Saha, P.K., Gomberg, B.R., Song, H.K., Snyder, P.J., Benito, M., Wright, A. & Weening, R. (2002). Role of Magnetic Resonance for Assessing Structure and Function of Trabecular Bone. *Top Magn. Reson. Imaging* **13**, 335-355.

Weinkamer, R., Hartmann, M. A., Brechet, Y. & Fratzl, P. (2004). Stochastic Lattice Model for Bone Remodeling and Aging. *Phys. Rev. Lett.* **93**, 228102.

Weinkamer, R., Hartmann, M.A., Brechet, Y. & Fratzl, P. (2005). Architectural Changes of Trabecular Bone Caused by the Remodeling Process. In *Mater. Res. Soc. Symp. Proc. 874*, L1.9.

Zaikin, A., Saparin, P., Kurths, J., Prohaska, S. & Gowin, W. (2005) Modelling Bone Resorption in 2D CT and 3D μCT Images. *Int. J. Bifurcat. Chaos*; in Press.

Zerath, E., Godet, D., Holy, X., Andre, C., Renault, S., Hott, M. & Marie, P.J. (1996). Effects of Spaceflight and Recovery on Rat Humeri and Vertebrae: Histological and Cell Culture Studies. *J. Appl. Physiol.* **81**, 164-171.

Zurek, W.H. (Ed.) (1990). *Complexity, Entropy and the Physics of Information*, Santa Fe Institute Studies in the Sciences of Complexity, Addison Wesley Publishing.

MAP Team Members

Academic Partners
Dr. Peter Saparin
Max Planck Institute of Colloids and Interfaces, Department of Biomaterials, Research Campus Golm, D-14424 Potsdam, Germany.
Tel: +49 331 567 9446
Fax: +49-331 567 9402
Email: peter.saparin@mpikg-golm.mpg.de

Dr. Wolfgang Gowin
Hunter Imaging Group, P.O.Box 192, New Lambton NSW 2305, Australia.
Email: wolfgang.gowin@bigpond.com

Prof. Dr. Peter Fratzl
Max Planck Institute of Colloids and Interfaces, Department of Biomaterials, Research Campus Golm, D-14424 Potsdam, Germany.
Tel: +49 331 567 9401
Fax: +49 331 567 9402
Email: peter.fratzl@mpikg-golm.mpg.de

Dr. Richard Weinkamer
Max Planck Institute of Colloids and Interfaces, Department of Biomaterials, Research Campus Golm, D-14424 Potsdam, Germany.
Tel: +49 331 567 9410
Fax: +49 331 567 9402
Email: richard.weinkamer@mpikg-golm.mpg.de

Prof. Dr. Dieter Felsenberg
Center of Muscle and Bone Research, Dept. of Radiology, Charité – University Medicine Berlin, Campus Benjamin Franklin, Hindenburgdamm 30, D-12200 Berlin, Germany.
Tel: +49 30 8445 3046
Fax: +49 30 8440 9942
Email: dieter.felsenberg@charite.de

Gisela Beller
Center of Muscle and Bone Research, Dept. of Radiology, Charité – University Medicine Berlin, Campus Benjamin Franklin, Hindenburgdamm 30, D-12200 Berlin, Germany.
Tel: +49 30 8445 4617
Fax: +49 30 8445 4539
Email: gise.beller@charite.de

Dr. Jesper Skovhus Thomsen
Dept. of Connective Tissue Biology, Institute of Anatomy, University of Aarhus, DK-8000 Århus, Denmark.
Tel: +45 8942 3015
Fax: +45 8613 7539
Email: jesper@jst.ana.au.dk

Dr. Lis Mosekilde
Institute of Anatomy, University of Aarhus, DK-8000 Århus, Denmark.
(deceased, 18 June 2002)

Prof. Dr. Jürgen Kurths
Nonlinear Dynamics Group, Institute of Physics, University of Potsdam, Am Neuen Palais 10, D-14415 Potsdam, Germany.
Tel: +49 331 977 1429
Fax: +49 331 977 1142
Email: jkurths@agnld.uni-potsdam.de

Dr. Norbert Marwan
Nonlinear Dynamics Group, Institute of Physics, University of Potsdam, Am Neuen Palais 10, D-14415 Potsdam, Germany.
Tel: +49 331 977 1302
Fax: +49 331 977 1142
Email: marwan@agnld.uni-potsdam.de

Hon.-Prof. Hans-Christian Hege
Zuse Institute Berlin (ZIB), Takustrasse 7, D-14195 Berlin, Germany.
Tel: +49 30 841 85 141
Fax: +49 30 841 85 107
Email: hege@zib.de

Steffen Prohaska
Zuse Institute Berlin (ZIB), Takustrasse 7, D-14195 Berlin, Germany.
Tel: +49 30 841 85 337
Fax: +49 30 841 85 107
Email: prohaska@zib.de

Dr. Alexey Tatarinov
Riga Technical University, Kalku 1, Riga, LV-1050, Latvia.
Tel: +371 755 87 73
Fax: +371 755 87 37
Email: alta2003@apollo.lv

Industrial Partners
Dr. Bruno Koller
Scanco Medical AG, Auenring 6-8, CH-8303 Bassersdorf, Switzerland.
Tel: +41 1 837 0710
Fax: +41 1 837 0713
Email: bkoller@scanco.ch

Mr. Christian Asbeck
Siemens Medical Solutions, Siemensstraße 1, D-91301 Forchheim, Germany.
Tel: +49 9191 18-8211
Fax: +49-9191 18-8340
Email: christian.asbeck@siemens.com

Dr. Malte Westerhoff
Mercury Computer Systems GmbH, Lepsiusstr. 70, D-12163 Berlin, Germany.
Tel: +49 30 700 968 22
Fax: +49 30 700 968 11
Email: mwesterh@mc.com

European Space Agency
Agence spatiale européenne

Contact: ESA Publications Division
c/o ESTEC, PO Box 299, 2200 AG Noordwijk, The Netherlands
Tel. (31) 71 565 3400 - Fax (31) 71 565 5433